

# Fluid dynamic insights into virus deposition and transport in the deep lung

Aranyak Chakravarty<sup>a</sup>, Mahesh V. Panchagnula<sup>b</sup>, Neelesh A. Patankar<sup>c,\*</sup>

<sup>a</sup>*School of Nuclear Studies & Application, Jadavpur University, Kolkata, India*

<sup>b</sup>*Department of Applied Mechanics, Indian Institute of Technology Madras, Chennai, India*

<sup>c</sup>*Department of Mechanical Engineering, Northwestern University, Evanston, IL, USA*

---

## Abstract

The primary mode of respiratory virus transmission is by means of virus-laden aerosols. The aerosols are inhaled into the respiratory tract and deposited in the mucosa, where the virus may interact with the epithelial tissue causing infection. Transport of virus within the respiratory tract and clearance from the lungs, as such, becomes extremely important. This phenomena is mathematically modelled using a coupled model of aerosol transport and virus transport within a Weibel-like idealisation of the lung geometry. The analysis is carried out in a dimensionless manner and the results are presented in terms of various dimensionless parameters. It is observed that the main factor determining virus transport and clearance from the lungs is the region where the virus-laden aerosols are deposited within the lungs. Viruses deposited in the upper respiratory tract are cleared out of the lung relatively faster due to the impact of mucociliary clearance. Viruses deposited in the deep lung are cleared much slowly due to absence of mucociliary clearance. Deep lung deposition is observed to take place for a specific range of aerosol sizes. Slower breathing and deep breaths is observed to promote deep lung deposition. Slower breathing and larger mucus clearance is also observed to enhance virus clearance from the upper respiratory tract. It is further observed that virus clearance from the deep lung can only be enhanced by increasing virus diffusivity. This enhancement is, however, not substantial. It is, thus, essential to eliminate the situations which promote deep lung deposition of the viruses.

*Keywords: aerosol transport, virus deposition, mucociliary clearance, virus transport, mathematical modelling*

---

## 1. Introduction

Respiratory viruses (for e.g. SARS-CoV2) are transmitted mainly through virus-laden droplets and aerosols [1]. These are formed within the respiratory tract of an infected individual, expelled into the environment by various mechanisms (talking, sneezing, coughing and even normal exhalation) and can be subsequently inhaled by other individuals. Once inhaled, the droplets/aerosols travel along the respiratory tract following breathing dynamics and are deposited in the respiratory mucosa through different mechanisms [2]. The mucosa, fortunately, provides a certain level of inherent protection of the respiratory tract from the deposited viruses [3]. As such, inhalation and deposition of virus-laden droplets/aerosols does not always lead to infection of the individual. Even when an individual does get infected, they may remain asymptomatic or exhibit mild symptoms in certain cases, while major health complications such as pneumonia are also possible. Such variation in symptoms could be a manifestation of the interaction of the viruses with the mucosa. It can also depend on the transport of the deposited viruses within the respiratory tract. No definite answer is, however, yet available and hence, requires much more detailed analysis. The present article attempts to computationally analyse the latter - deposition and transport of viruses within the respiratory tract - through a coupled analysis of aerosol and virus transport within the lungs.

Research has established that the transport of aerosols in the respiratory system is governed by the combined effects of unsteady convective air flow, gravitational settling, and diffusion motion of the aerosols

---

\*Corresponding author

*Email address:* n-patankar@northwestern.edu (Neelesh A. Patankar)

within air. The inhaled aerosols travel along the respiratory tract during which they are exposed to different physical mechanisms. The aerosols are forced to leave the airflow streamlines as a result of such exposures leading to their deposition in the mucosa. The principal deposition mechanisms have been observed to be diffusion, sedimentation and inertial impaction [2, 4, 5]. While inertial impaction remains significant in the upper airways, sedimentation and diffusion becomes the dominant mechanisms in the deeper airways [4]. The extent of influence of these mechanisms is determined by the size, shape and distribution of the aerosols as well as the breathing pattern (tidal volume, breathing frequency, air flow rate etc) and morphology of the respiratory tract [5].

Computational modelling of aerosol transport and deposition in the respiratory tract has been carried out using different techniques [5]. Both Eulerian and Lagrangian approaches have been used for such modelling. Some of these models consider localised regions of the lung for analysis. Such localised models may range from a single airway to bifurcating channels and even a branching network comprising a few lung generations [6, 7, 8]. At the other extremity are *whole lung* models which consider the lung to be a network of interconnected branching channels with varying dimensions. Such *whole lung* models include semi-empirical regional compartment models [9], one-dimensional *trumpet* models [10, 11] and various mechanistic models [5]. A common requirement in all *whole lung* models is an assumption of the lung morphometry. The most widely used lung morphometric model is the Weibel model [12] which is based upon detailed morphometric data of the branching lung geometry. Other such models include the ones proposed by Yeh and Schaum [13] and Horsfield and Cumming [14] among various others.

The respiratory mucosa acts a barrier between the airway lumen and the epithelial tissue lining the respiratory tract (see Fig. 1). The aerosols deposited in the mucosa, therefore, faces resistance in coming into contact with the epithelial cells. The mucosa comprises of two liquid sub-layers - the mucus layer lining the airway lumen and the periciliary layer beneath it [15]. The epithelium is also lined with cilia that beats metachronously within the periciliary layer [16]. This beating mechanism displaces the mucus from the distal regions of the lung towards the top of the trachea, where it is either swallowed or expectorated. Such mucociliary transport, as such, provides a natural defence of the lungs against foreign particles in general and viruses, in particular. It is, thus, essential to consider the mucociliary transport while analysing virus transport in the lungs. Mathematical models of virus spread in respiratory tracts generally take into account infection kinetics that describes the temporal evolution of virus spread. A large volume of work has been carried out in evaluating virus spread and localisation using these models through various approaches [17, 18, 19]. However, only a few have taken into consideration the impact of virus diffusion in the mucus and mucociliary clearance on virus spread in the respiratory tract. Quirouette et al. [3] evaluated the spread and localisation of Influenza A virus in the human respiratory tract using one such model. They observed that virus diffusion has negligible effects as compared to mucociliary transport which effectively clears the lungs of the virus. Infection, as such, peaks and resolves faster in the upper respiratory tract than the lower tract. However, they considered only a portion of the upper respiratory tract in their analysis and not the whole lung.

None of these mathematical models for virus spread, however, have considered aerosol transport and deposition models, although these processes occur simultaneously with virus spread within the lung. The time-scale of virus transport is much slower than the corresponding time-scale of aerosol transport and deposition. A coupled model of aerosol transport, deposition and virus transport, thus, becomes necessary to fully account for the transport phenomena within the lungs. The present article reports the development of a coupled mathematical model of aerosol and virus transport within a Weibel-like one-dimensional model of the human lung. Aerosol deposition is estimated using appropriate empirical models and converted to a suitable form that fits with the derived mathematical model. It is also assumed that airflow within the lungs and aerosol transport remains de-coupled. This is possible due to the time-periodic nature of airflow and aerosol transport [6], and helps eliminating the need for solving the airflow equations explicitly. The mathematical model is reduced to a dimensionless form using suitable scaling parameters and is used to study the impact of pertinent dimensionless parameters on virus transport within the lung.

## 2. Mathematical Modelling

### 2.1. Idealisation of the lung geometry

The lung geometry considered in this analysis is an idealisation of the physiological network of airways and alveoli that is encountered in a real lung. Physiological investigations have estimated that a real human lung can be subdivided into approximately 24 generations based on bifurcation of the bronchioles, with distinct length and cross-sectional areas of each generation [12]. Number of bronchioles in each generation is estimated as  $2^N$ , where  $N$  is the generation number. Further, investigations have revealed that airways are alveolated from generation 17 onwards with increasing alveolation as one moves deeper down the generations.

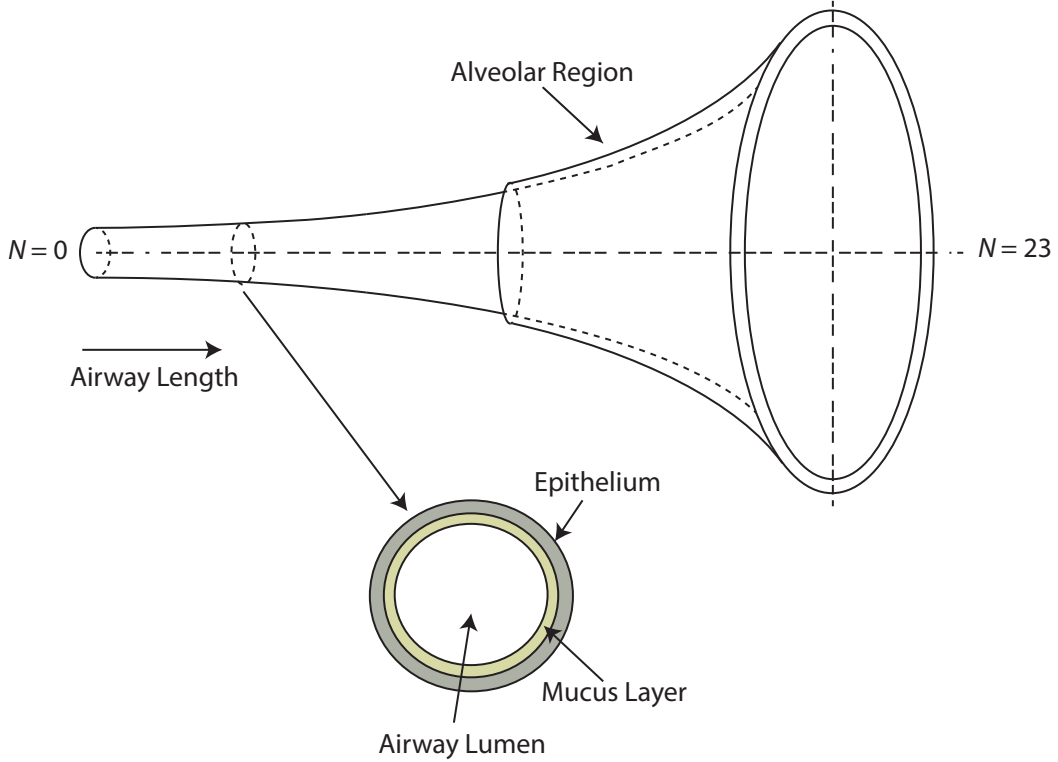


Figure 1: Schematic illustration of the one-dimensional *trumpet* model of the human lungs

The lung geometry considered in the present analysis is a one-dimensional approximation of the system of airways and alveoli encountered in a real human lung. The airway is modelled as a continuous one-dimensional channel of variable cross-sectional area and length divided into 24 generations ( $N = 0 - 23$ ). The length ( $L$ ) and cross-sectional area ( $A$ ) of each generation ( $N$ ) is calculated using a power-law function as

$$L_N = L_0 \alpha^N \quad (1)$$

$$A_N = A_0 (2\beta)^N \quad (2)$$

where,  $L_0$  and  $A_0$  represents the length and cross-sectional area at  $N = 0$ , respectively (see Table 1 for magnitudes). The quantities  $\alpha$  and  $\beta$  are defined as the length-change and area-change factors, respectively. The magnitudes of  $\alpha$  and  $\beta$  are selected (see Table 1) such that the computed length and area matches the experimentally observed magnitudes as closely as possible [12].

Figure 1 schematically represents the modelled system of airways and alveoli. Alveolation of the airways is considered from generation 17 onwards as in a real human lung. Table 2 lists the fractions of the airway area that is assumed to be alveolated in different generations. The modelled system of airways and alveoli is also assumed to be lined by a thin mucus layer which has a uniform advective motion from the deeper

Table 1: Parameters used in modelling the lung geometry

$L_0$	0.12 m [12]	$\alpha$	0.73
$A_0$	0.000317m <sup>2</sup> [12]	$\beta$	0.71
$R_0$	$\sqrt{A_0/\pi}$	$\zeta$	0.9
$\delta_0$	10 $\mu$ m [16]	$\varepsilon$	0.87
$A_{m,0}$	$2\pi R_0\delta_0$		
$V_{m,0}$	-5 mm/min [16]		

Table 2: Fractions of alveolated airways in different generations [22]

Lung Generation ( $N$ )	Fraction of alveolated area ( $\gamma$ )
0-16	0
17	0.0011
18	0.0041
19	0.0135
20	0.0509
21	0.1168
22	0.2712
23	0.5424

generations towards the 0<sup>th</sup> generation. Thickness of the mucus layer as well as the advective motion of the mucus due to mucociliary transport is assumed to be temporally invariant in this analysis [16]. Thickness ( $\delta$ ) and area of mucus layer ( $A_m$ ), and the advective mucus velocity due to mucociliary transport ( $V_m$ ) at different lung generations are also estimated using a power-law function as

$$\delta_N = \delta_0 \zeta^N \quad (3)$$

$$A_{m,N} = A_{m,0} (2\sqrt{\beta}\zeta)^N \quad (4)$$

$$\begin{aligned} V_{m,N} &= V_{m,0} \varepsilon^N, \text{ for } N < 18 \\ &= 0, \text{ for } N \geq 18 \end{aligned} \quad (5)$$

where,  $\delta_0$ ,  $A_{m,0}$  and  $V_{m,0}$  are the mucus thickness, area and velocity at  $N = 0$ , respectively (see Table 1 for magnitudes). The magnitudes of  $\zeta$  and  $\varepsilon$  used in this analysis are also listed in Table 1. Note that the mucus velocity due to mucociliary transport is considered only till  $N = 18$  (Eq. 5) due to absence of any appreciable mucociliary transport in the deep lung [20, 21].

## 2.2. Aerosol transport

The 1D transport equation for the aerosol particles in the idealised lung geometry is expressed in Eq.6. It is based on the *trumpet* model proposed by Taulbee & Yu [10] and later used by various authors to study various aspects of aerosol deposition in the lung [11, 23, 24]. The transport equation is formulated based on the assumption that the aerosol particles are monodispersed, do not undergo coagulation and are decoupled from airflow in the lungs. It is also assumed that external forces (such as electrical and magnetic forces) do not have any influence on the aerosol particle dynamics. It is further assumed that there is no additional source of aerosols present within the lungs and the aerosols are either deposited in the airway mucus or washed out of the airways.

$$\frac{\partial(A_N c_{ae,N})}{\partial t} + \frac{\partial(Q c_{ae,N})}{\partial x} = \frac{\partial}{\partial x} (A_N D_{ae} \frac{\partial c_{ae,N}}{\partial x}) - L_{dep} c_{ae} \quad (6)$$

where,  $c_{ae}$  represents the aerosol concentration,  $Q$  represents the volume flow rate of air in breathing and  $D_{ae}$  represents the diffusivity of aerosols in air. The term  $L_{dep}$  accounts for the aerosols deposited in the

airway mucus.

Equation 6 is represented in terms of airway length ( $x$ ), while the lung model adopted is in terms of lung generation number ( $N$ ). As such, Eq. 6 needs to be converted to a more appropriate form in terms of  $N$ . This requires an additional mathematical relation (Eq. 7) connecting airway length  $x$  and the lung generation number ( $N$ ).

$$\frac{\partial N}{\partial x} = -\frac{1-\alpha}{L_0\alpha \ln(\alpha)\alpha^N} \quad (7)$$

Converting Eq.6 using Eqs. 7 and 2, we get -

$$A_0(2\beta)^N \frac{\partial c_{ae,N}}{\partial t} = \frac{\partial N}{\partial x} \frac{\partial}{\partial N} \left[ \left( A_0(2\beta)^N D_{ae} \frac{\partial N}{\partial x} \frac{\partial c_{ae,N}}{\partial N} \right) - \left( Q_{max} q(t) c_{ae,N} \right) \right] - L_{dep} c_{ae} \quad (8)$$

where,  $q(t)$  represents the temporal function accounting for airflow variation such that  $Q = Q_{max}q(t)$ . Equation 8 is reduced to its dimensionless form by multiplying and dividing Eq. 8 with  $\left( \frac{L_0}{A_0 D_{ae}} \right)$  and  $\left( -\frac{\alpha \ln(\alpha)}{1-\alpha} \right)$ , respectively, and using the following parameters -

$$\tau = \frac{t}{T_b}, \phi_{ae,N} = \frac{c_{ae,N}}{c_{ae,0}}, T_a = \frac{L_0 A_0}{|Q_{max}|}, St_a = \frac{T_a}{T_b}, |Pe_{ae,max}| = \frac{|Q_{max}| L_0}{A_0 D_{ae}}, D_{ae} = \frac{k_B T C_s}{6\pi \mu_{air} r_{ae}} \quad (9)$$

where,  $Pe_{ae}$  and  $St_a$  represents the Peclet number for the aerosols and Strouhal number for the airways, respectively.  $\phi_{ae}$  and  $\tau$  denotes the dimensionless aerosol concentration and time, respectively, while the quantities  $T_a$  and  $T_b$  represents the convective airflow time-scale and breathing time-scale, respectively. The expression of  $D_{ae}$  is based on the Stokes-Einstein relation [6] where  $C_s$  represents the Cunningham slip correction,  $T$  represents the ambient temperature,  $\mu_{air}$  denotes air viscosity and  $r_{ae}$  denotes the aerosol size.

The dimensionless equation, thus, obtained is used to analyse aerosol transport in the present study and is expressed as -

$$|Pe_{ae,max}| St_a (2\alpha\beta)^N \frac{\partial(\phi_{ae,N})}{\partial \tau} = \frac{\partial}{\partial N} \left[ \left( \left( \frac{2\beta}{\alpha} \right)^N \left( \frac{1-\alpha}{\alpha \ln(\alpha)} \right)^2 \frac{\partial \phi_{ae,N}}{\partial N} \right) + \left( |Pe_{ae,max}| q(t) \left( \frac{1-\alpha}{\alpha \ln(\alpha)} \right) \phi_{ae,N} \right) \right] - L'_{dep} \phi_{ae} \quad (10)$$

where,  $L'_{dep}$  represents the dimensionless form of the aerosol deposition ( $L_{dep}$ ) and is expressed as

$$L'_{dep} = L_{dep} \frac{L_0^2}{A_0 D_{ae}} \alpha^N \quad (11)$$

### 2.3. Aerosol deposition models

The major mechanisms of aerosol deposition in the lungs have been identified in the literature as diffusion, sedimentation and impaction of the aerosols in the airways, as well as diffusion and sedimentation in the alveoli [5, 11]. Different empirical models have been used to estimate the different depositions. However, these models need to be converted into a more appropriate form for use in the present analysis.

The probability of aerosol deposition in the airways by diffusion ( $P_d$ ), sedimentation ( $P_s$ ) and impaction ( $P_i$ ) can be expressed following Yeh & Schaum [13] as

$$\frac{c_{ae,0} - c_{ae}}{c_{ae,0}} = P_d + P_s + P_i - P_d P_s - P_d P_i - P_s P_i - P_d P_s P_i \quad (12)$$

On algebraic manipulation, Eq. 12 can be re-written as

$$\begin{aligned} \frac{c_{ae}}{c_{ae,0}} &= (1 - P_d)(1 - P_s)(1 - P_i) = \left( \sum C_{d,n} e^{-k_{d,n}x} \right) (C_s e^{-k_s x}) (C_i e^{-k_i x}) \\ &\implies c_{ae} = c_{ae,0} \sum \left[ C_{d,n} C_s C_i e^{-(k_{d,n} + k_s + k_i)x} \right] \end{aligned} \quad (13)$$

Taking the derivative of Eq. 13 with respect to  $x$ , we obtain -

$$\frac{dc_{ae}}{dx} = -c_{ae,0} \sum \left[ (k_{d,n} + k_s + k_i) C_{d,n} C_s C_i e^{-(k_{d,n} + k_s + k_i)x} \right] = -(k_{d,n} + k_s + k_i) C_{ae} \quad (14)$$

Equation 14 represents the aerosol deposition flux in the airways. It is further converted to a dimensionally relevant form for use in the transport equation (Eq. 8) as follows -

$$\frac{D(Ac_{ae})}{Dt} \simeq Av \frac{dc_{ae}}{dx} = -Av(k_{d,n} + k_s + k_i) C_{ae} = L_{dep} c_{ae} \implies L_{dep} = Av(k_{d,n} + k_s + k_i) \quad (15)$$

The empirical relations for the different deposition mechanisms are converted to a form relevant to Eq. 15 and then reduced to their dimensionless forms for use in the final transport equation (Eq. 10).

### 2.3.1. Diffusional deposition in the airways

The probability of diffusional deposition of the aerosols in the airways is expressed following Yeh & Schaum [13] as

$$P_d = 1 - 0.819e^{-7.315x} - 0.0976e^{-44.61x} - 0.0325e^{-114x} \quad (16)$$

On linearisation of the above equation following Eq. 13, we obtain -

$$k_{d,1} = 7.315 \frac{D_{ae}}{2R_N^2 v_N}, k_{d,2} = 44.61 \frac{D_{ae}}{2R_N^2 v_N}, k_{d,3} = 114 \frac{D_{ae}}{2R_N^2 v_N} \quad (17)$$

and

$$k_d = k_{d,1} + k_{d,2} + k_{d,3} = (7.315 + 44.61 + 114) \frac{D_{ae}}{2R_N^2 v_N} \quad (18)$$

where,  $R_N$  and  $v_N$  denotes the airway radius and airflow velocity of a respective lung generation, respectively. Using this, aerosol deposition in the airways due to aerosol diffusion is estimated as

$$L_{dep,d} = v_N A_{N,T} k_d = v_N \pi R_N^2 2^N (7.315 + 44.61 + 114) \frac{D_{ae}}{2R_N^2 v_N} \quad (19)$$

Conversion of Eq. 19 to its dimensionless form gives us the following expression for dimensionless diffusional deposition of the aerosols in the airways -

$$L'_{dep,d} = L_{dep,d} \frac{L_0^2}{A_0 D_{ae}} \alpha^N = \left( \frac{L_0}{R_0} \right)^2 (2\alpha)^N (3.66 + 22.305 + 57) \quad (20)$$

### 2.3.2. Sedimentation deposition in the airways

The probability of deposition of the aerosols due to sedimentation in the airways is expressed following Yeh & Schaum [13] as

$$P_s = 1 - \exp \left[ - \left( \frac{4gC_s \rho_{ae} r_{ae}^2 \cos(\psi_N)}{9\pi \mu_{air} R_N v_N} x \right) \right] \quad (21)$$

where,  $\rho_{ae}$ ,  $g$  and  $\psi$  represents aerosol density, gravitational acceleration and airway orientation angle considering horizontal as  $90^\circ$ , respectively. Linearising the above equation using the approach followed in Eq.13, we obtain -

$$k_s = \frac{4gC_s\rho_p r_p^2 \cos(\psi_N)}{9\pi\mu_{air}R_N v_N} \quad (22)$$

Aerosol deposition in the airways due to sedimentation can, then, be estimated as -

$$\begin{aligned} L_{dep,s} &= v_N A_{N,T} k_s = v_N (\pi R_N^2 2^N) \frac{4gC_s\rho_p r_p^2 \cos(\psi_N)}{9\pi\mu_{air}R_N v_N} \\ &= \frac{4}{9} \frac{R_N g C_s \rho_p r_p^2 \cos(\psi_N)}{\pi\mu_{air}} 2^N \end{aligned} \quad (23)$$

Conversion of the dimensional deposition ( $L_{dep,s}$ ) to its dimensionless form gives us the following expression for dimensionless sedimentation deposition in the airways -

$$L'_{dep,s} = L_{dep,s} \frac{L_0^2}{A_0 D_{ae}} \alpha^N = \frac{8}{3} \left( \frac{L_0}{R_0} \right)^2 (2\alpha\sqrt{\beta})^N S_g \cos(\psi_N) \quad (24)$$

where,  $S_g$  is defined as the sedimentation parameter and expressed as

$$S_g = \frac{R_0 \rho_p r_p^3 g}{k_B T} \quad (25)$$

### 2.3.3. Impact deposition in the airways

The probability of deposition due to impaction of the aerosols in the airways is given by Yeh & Schaum [13] as

$$P_i = 1 - f_i(\theta, St) \quad (26)$$

where,  $\theta$  denotes the branching angle of the airways and  $St$  denotes the Stokes number ( $= \frac{C_s \rho_p r_p^2 v_N}{9\mu_{air} R_N}$ ). The function  $f_i(\theta, St)$  is expressed as follows -

$$\begin{aligned} f_i(\theta, St) &= \frac{2}{\pi} \cos^{-1}(\theta \cdot St) - \frac{1}{\pi} \sin \left[ 2 \cos^{-1}(\theta \cdot St) \right] \text{ for } \theta \cdot St < 1 \text{ (Inhalation)} \\ &= 1 \text{ for } \theta \cdot St \geq 1 \text{ (Exhalation)} \end{aligned} \quad (27)$$

The expression of  $P_i$  is not in a form that can be directly linearised. As such, certain mathematical treatments need to be carried out in order to estimate the impact deposition. Loss of aerosols in one generation of the lungs can be determined based on the aerosol concentrations before and after the lung generation. Mathematically, this can be expressed as

$$\begin{aligned} \text{Loss in a generation} &= \frac{C_{bef} - C_{aft}}{C_{bef}} = 1 - f_i(\theta, St) \\ \implies \frac{C_{aft}}{C_{bef}} &= f_i(\theta, St) \end{aligned} \quad (28)$$

In terms of lung generations, the above expression can be re-written as

$$C_N = f_i^N(\theta, St) C_0 \quad (29)$$

Differentiating with respect to generation number, we obtain -

$$\frac{dC_N}{dN} = C_0 \ln(f_i^N(\theta, St)) f_i^N(\theta, St) = \ln(f_i^N(\theta, St)) C_N \quad (30)$$

Converting the above derivative to a derivative in terms of  $x$ , we get -

$$\begin{aligned}\frac{dC(x)}{dx} &= -(-\ln(f_i^N(\theta, St)))\frac{dN}{dx}C(x) \\ \implies k_i &= (-\ln(f_i^N(\theta, St)))\frac{dN}{dx}\end{aligned}\quad (31)$$

The impact deposition is estimated using the above expression as

$$L_{dep,i} = v_N A_{N,T} k_i = v_N \pi R_N^2 2^N (-\ln(f_i^N(\theta, St)))\frac{dN}{dx}\quad (32)$$

The dimensionless form of the impact deposition is obtained following a similar approach as in Sections 2.3.1 and 2.3.2. The dimensionless impact deposition, thus, obtained is expressed as

$$L'_{dep,i} = L_{dep,i} \frac{L_0^2}{A_0 D_{ae}} \alpha^N = |Pe_{ae,max}| q(t) \ln(f_i^N(\theta, St)) \frac{(1-\alpha)}{\alpha \ln(\alpha)}\quad (33)$$

#### 2.3.4. Diffusional deposition in the alveoli

Diffusional deposition of the aerosols in the alveoli is estimated using the following dimensionless expression -

$$L'_{dep,d,alv} = \gamma_N \eta_{d,alv} |Pe_{ae,max}| q(t) \left( \frac{1-\alpha}{-\alpha \ln(\alpha)} \right)\quad (34)$$

where,  $\gamma_N$  denotes the fraction of alveolated area in the corresponding generation (see Table 2) and  $\eta_{d,alv}$  denotes the diffusional deposition efficiency in the alveoli.  $\eta_{d,alv}$  is expressed as [11]

$$\eta_{d,alv} = 1 - \frac{6}{\pi^2} \sum \frac{1}{k^2} \exp \left[ -\frac{4k^2 t D_{ae}}{d_{eq}^2} \right]\quad (35)$$

#### 2.3.5. Sedimentation deposition in the alveoli

Deposition of the inhaled aerosols due to their sedimentation in the alveoli are estimated using the following dimensionless expression -

$$L'_{dep,s,alv} = \gamma_N \eta_{s,alv} |Pe_{ae,max}| q(t) \left( \frac{1-\alpha}{-\alpha \ln(\alpha)} \right)\quad (36)$$

where,  $\gamma_N$  and  $\eta_{s,alv}$  denotes the fraction of alveolated area in the corresponding generation (see Table 2) and sedimentation deposition efficiency in the alveoli, respectively.  $\eta_{s,alv}$  is expressed as [11]

$$\eta_{s,alv} = \left[ 1 + \min \left( \frac{d_s}{d_{eq}}, 1 \right) \right]^2 \left[ 1 - 0.5 \min \left( \frac{d_s}{d_{eq}}, 1 \right) \right]^2 - 1\quad (37)$$

#### 2.4. Virus transport

The corresponding 1D transport equation for the virus particles in the airway mucus is expressed as

$$\frac{\partial(A_{m,N} c_{vi,N})}{\partial t} + \frac{\partial(Q_m c_{vi,N})}{\partial x} = \frac{\partial}{\partial x} (A_{m,N} D_{vi} \frac{\partial c_{vi,N}}{\partial x}) + Source\quad (38)$$

where,  $c_{vi}$  denotes the virus concentration in the airway mucus,  $Q_m$  represents the volume flow rate of mucociliary clearance and  $D_{vi}$  denotes the diffusivity of viruses in the mucus layer.

The virus-laden aerosols deposited in the airway mucus serve as the only source of virus in the lungs. The *Source* term in Eq. 38 is, therefore, equivalent in magnitude to the deposition term in Eq. 6 ( $L_{dep,ae}$ ) times the *viral load* ( $\phi_l$ ). Mathematically, this is expressed as -

$$Source = L_{dep,ae} \phi_l\quad (39)$$



where,  $\phi_l$  is defined as the quantity of virus contained by the aerosols per unit quantity of the aerosol. Equation 38 is converted to a form in terms of  $N$  using Eqs. 7 and 4 in a similar manner as in Section 2.2 as follows -

$$A_{m,0}(2\zeta\sqrt{\beta})^N \frac{\partial x}{\partial N} \frac{\partial c_{vi,N}}{\partial t} = \frac{\partial}{\partial N} \left[ \left( A_{m,0}(2\zeta\sqrt{\beta})^N D_{vi} \frac{\partial c_{vi,N}}{\partial N} \right) - \left( Q_{m,0}(2\varepsilon\zeta\sqrt{\beta})^N c_{vi,N} \right) \right] + (\phi_l L_{dep} c_{ae}) \frac{\partial x}{\partial N} \quad (40)$$

The above equation is further reduced by multiplying and dividing by  $\left(\frac{L_0}{A_{m,0}D_{vi}}\right)$  and  $\left(-\frac{\alpha \ln(\alpha)}{1-\alpha}\right)$ , respectively. The reduced equation is expressed as

$$\frac{L_0|V_{m,0}|}{D_{vi}}(2\alpha\zeta\sqrt{\beta})^N \frac{T_m}{T_b} \frac{\partial c_{vi,N}}{\partial t} = \frac{\partial}{\partial N} \left[ \left( \left( \frac{2\zeta\sqrt{\beta}}{\alpha} \right)^N \left( \frac{1-\alpha}{\alpha \ln(\alpha)} \right)^2 \frac{\partial c_{vi,N}}{\partial N} \right) - \left( \frac{L_0|V_{m,0}|}{D_{vi}}(2\varepsilon\zeta\sqrt{\beta})^N c_{vi,N} \right) \right] + \left( \phi_l L'_{dep} \frac{A_0 D_{ae}}{L_0^2 \alpha^N} \phi_{ae} c_{ae,0} \frac{L_0^2 \alpha^N}{A_{m,0} D_{vi}} \right) \quad (41)$$

The following parameters are utilised to achieve the dimensionless form of the virus transport equation in the airway mucus given by Eq. 43.

$$\tau = \frac{t}{T_b}, \phi_{vi,N} = \frac{c_{vi,N}}{c_{vi,0}}, c_{vi,0} = \phi_l c_{ae,0} \frac{A_0}{A_{m,0}}, T_m = \frac{L_0}{|V_{m,0}|}, St_m = \frac{T_m}{T_b}, |Pe_{vi,max}| = \frac{|V_{m,0}|L_0}{D_{vi}}, D_{vi} = \frac{k_B T}{6\pi\mu_m r_{vi}} \quad (42)$$

$$|Pe_{vi,max}|(2\alpha\zeta\sqrt{\beta})^N St_m \frac{\partial \phi_{vi,N}}{\partial \tau} = \frac{\partial}{\partial N} \left[ \left( \left( \frac{2\zeta\sqrt{\beta}}{\alpha} \right)^N \left( \frac{1-\alpha}{\alpha \ln(\alpha)} \right)^2 \frac{\partial \phi_{vi,N}}{\partial N} \right) - \left( |Pe_{vi,max}|(2\varepsilon\zeta\sqrt{\beta})^N \phi_{vi,N} \right) \right] + \left( L'_{dep} \frac{D_{ae}}{D_{vi}} \phi_{ae} \right) \quad (43)$$

where,  $\phi_{vi}$ ,  $Pe_{vi}$  and  $St_m$  represents the dimensionless virus concentration, Peclet number for viruses and Strouhal number for the mucus layer, respectively.  $T_m$  denotes the time-scale for mucociliary transport. Virus diffusivity ( $D_{vi}$ ) is estimated using the Stokes-Einstein relation where  $\mu_m$  represents mucus viscosity and  $r_{vi}$  represents virus size.

### 2.5. Initial and boundary conditions

The entire lung is assumed to have zero concentration of aerosols as well as virus i.e.  $\phi_{ae} = \phi_{vi} = 0$  at all generations initially ( $\tau = 0$ ). Boundary conditions need to be specified at the two extremes of the lung i.e. at  $N = 0$  and  $N = 23$  for both aerosol and virus transport equations. These are summarised below.

$$N = 0: \phi_{ae} = 1, \tau \leq \tau_{inhalation} \text{ (Inhalation)} \\ \phi_{ae} = 0, \tau > \tau_{inhalation} \text{ (Inhalation)}$$

$$\frac{\partial(\text{Total flux of aerosols})}{\partial N} = 0 \text{ (Exhalation)}$$

$$\frac{\partial(\text{Total flux of virus})}{\partial N} = 0 \text{ (Inhalation/Exhalation)}$$

$$N = 23: \text{Total flux of aerosols} = 0 \text{ (Inhalation/Exhalation)} \\ \text{Total flux of virus} = 0 \text{ (Inhalation/Exhalation)}$$

## 2.6. Implementation of the model and validation

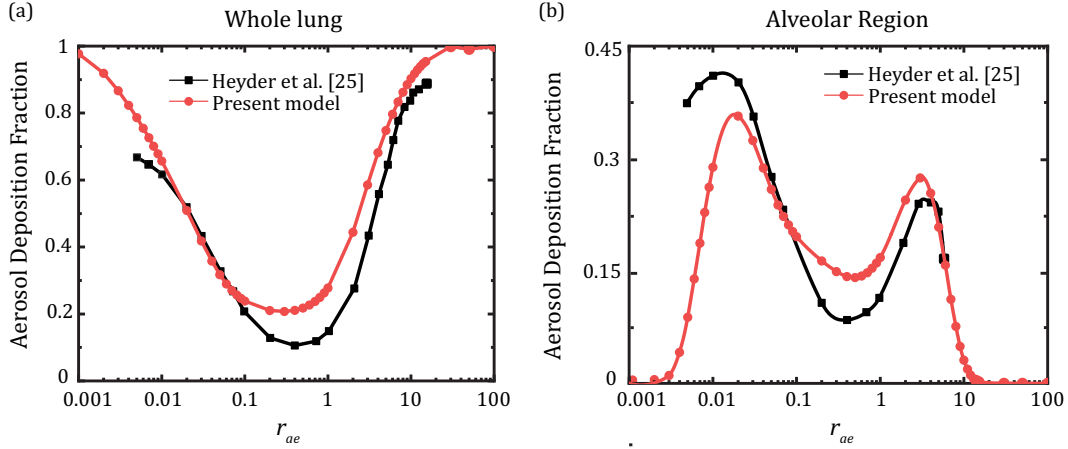


Figure 2: Comparison of the calculated aerosol deposition fraction for (a) the whole lung and (b) the alveolar region with the experimental results obtained by Heyder et al. [25]

The mathematical model discussed in Sections 2.2-2.4 is implemented for computational analysis using MATLAB<sup>®</sup>. The governing transport equations are discretised following the finite-difference technique with a first-order upwind and central-difference scheme used for the advective and diffusive terms, respectively. The temporal term is discretised using explicit forward differencing.

The implemented mathematical model is validated with respect to aerosol deposition within the lung - the most crucial aspect determining virus transport. Aerosol depositions predicted using the computational model are compared with the experimental data of Heyder et al. [25] with respect to deposition in the whole lung as well as deposition specifically in the alveolar region of the lung. The results are shown in Fig. 2. It can be observed that the computed aerosol deposition is in quite good agreement with the experimentally determined data.

## 3. Results

The results discussed in Sections 3.1 and 3.2 have been obtained using the following dimensionless parameters -  $Pe_{ae,max} = 2.85 \times 10^{10}$ ,  $Pe_{vi,max} = 4.56 \times 10^7$ ,  $St_a = 0.0095$ ,  $St_m = 359.7122$ , and  $\tau_{exp} = 5$ . Parametric studies for these parameters (Sections 3.3.1-3.3.5) have been carried out by varying the specific parameter only, while the other base parameters remain unchanged. It is assumed while obtaining the results that temporal airflow variation ( $q(t)$ ) during breathing follows a sinusoidal function.

### 3.1. Aerosol transport and deposition in the airways

Figure 3a represents the distribution of aerosol concentration within the adopted lung geometry at various instances of a breathing cycle for two different cases - with and without aerosol deposition in the airway mucus. It can be observed that, in either case, the aerosol concentration front gradually progresses into the deeper regions of the lung during inhalation part of the breathing cycle and reaches its extreme position at the end of inhalation. The reverse happens during exhalation with a substantial volume of the inhaled aerosols getting washed out of the lung. A comparison between the two cases, however, indicate substantial differences with respect to the location of the concentration front as well as its magnitude. The differences can be attributed to deposition of the aerosols in the airway mucus. It can be observed that the concentration fronts nearly overlap each other at the peak of inhalation, with the front for the deposition case located marginally behind that of the non-deposition case. With progress in the breathing cycle, more aerosols get deposited in the airways and the alveoli and hence, the gap between the two cases widen. As expected, the residual concentration of aerosols at the end of a breathing cycle is substantially less when deposition is considered. The deposition of aerosols in the airway mucus is shown in Fig. 3c with respect to the lung generations for the case when deposition is considered.

The impact of deposition on aerosol transport is also evident from a comparison of the aerosol washout curves between the two cases, as shown in Fig. 3b. The washout curves represent the temporal variation of aerosol concentration at the  $0^{th}$  generation of the lung. Aerosol concentration increases during inhalation, while it reduces during exhalation, for the duration of aerosol inhalation i.e. up to  $\tau = 5$ . Beyond that, the residual aerosols are quickly washed out of the lung. It can be observed that the nature of the washout curves are similar to that observed for gaseous transport in the lung. However, washout of the aerosols take place at a much faster rate as compared to the gases, which can be primarily attributed to the much smaller diffusivity of the aerosols in air.

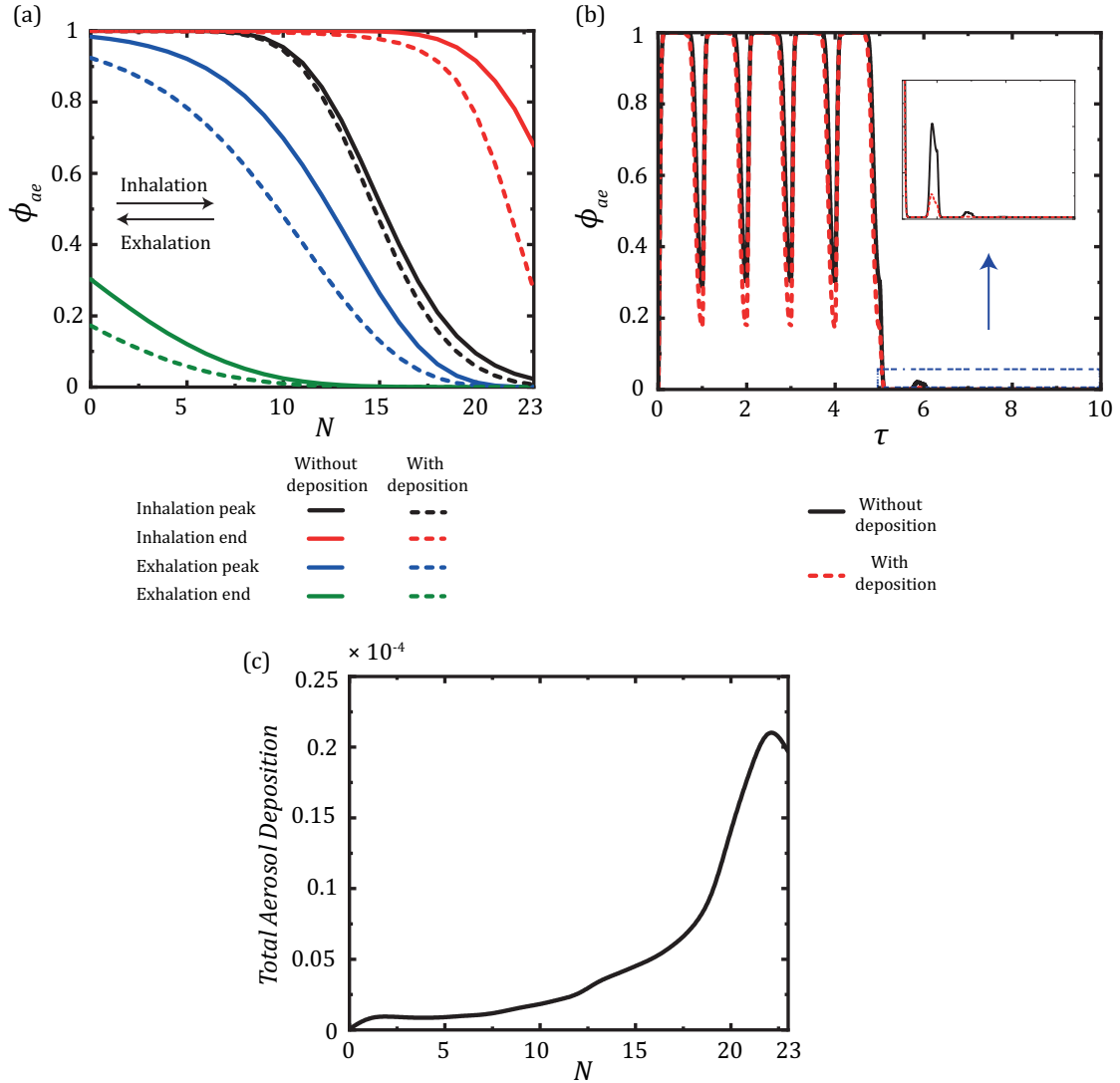


Figure 3: (a) Aerosol concentration with lung generations at different instances of a breathing cycle for two different cases - with and without aerosol deposition (b) Temporal change in aerosol concentration at the  $0^{th}$  generation of the lung with and without aerosol deposition (c) Aerosol deposition within the lung when deposition is considered. The results shown are for  $Pe_{ae} = 2.85 \times 10^{10}$  and  $St_a = 0.0095$ .

### 3.2. Virus transport in the airway mucus

The aerosols deposited in the airway mucus contribute as the only source of virus in the mucus layer. Aerosol deposition and the advective-diffusive transport of virus in the mucus are coupled processes, with aerosol deposition dominating over virus transport when aerosol inhalation is taking place. As such, virus

concentration in the mucus at the end of aerosol deposition (i.e. at  $\tau = 5$ ) qualitatively follows the aerosol deposition pattern (see Fig. 4a). However, virus transport - which occurs simultaneously with aerosol deposition - results in the deposited virus being transported away from the initial deposition location even as more virus is being deposited. This results in minor qualitative deviations between the virus concentration curve at  $\tau = 5$  and the aerosol deposition curve. The deviation is especially evident around  $N = 18$  as a result of the change in virus transport mechanism about this generation.

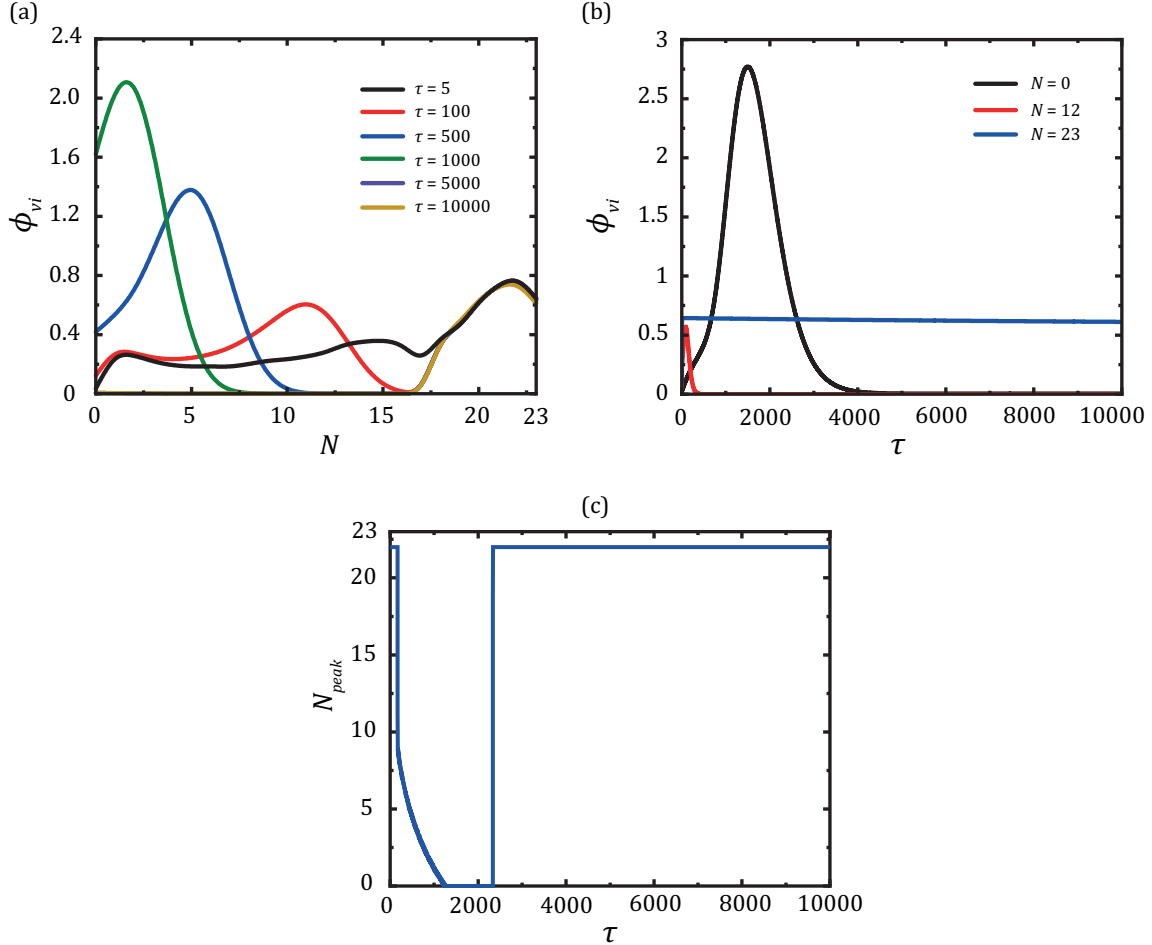


Figure 4: (a) Virus concentrations within the lung at different time instances (b) Temporal change in virus concentration at  $N = 0, 12, 23$  (c) Change in location of peak virus concentration within the lung with time. The results shown are for  $Pe_{ae} = 2.85 \times 10^{10}$ ,  $St_a = 0.0095$ ,  $Pe_{vi} = 4.56 \times 10^7$ ,  $St_m = 359.7122$ .

Viruses deposited in generation 18 onwards are transported purely by diffusion of the viruses, while the viruses deposited from generation 0 to 18 are transported through the combined action of advection of the mucus layer and diffusion of the viruses. Advective motion of the mucus layer, however, is much stronger as compared to the weak diffusive transport of the viruses within the mucus. The latter is a consequence of the small diffusivity of the viruses in mucus. The difference in the strength of transport results in a sharp change in virus concentration as observed at  $N = 18$ .

Viruses deposited before  $N = 18$  are transported towards the  $0^{th}$  generation and ultimately cleared out of the lung primarily as a result of the advective motion of the mucus layer. It is evident from Fig. 4a that the viruses - being transported from the higher to lower generations - result in accumulation in the lower generations leading to gradually larger concentration in the lower generations (due to smaller volume) as time progresses, before clearing out of the lung. The temporal change in virus concentration at the  $0^{th}$  generation in Fig. 4b also corroborates this.

Viruses deposited beyond generation 18 are not subjected to this clearance due to lack of advective motion in that region. Virus concentration in this region, therefore, undergoes very slow change as can be expected in a situation with very weak diffusive transport. As such, viruses deposited in this region of the lung remains stuck there for a much longer time as compared to those deposited before generation 18. This is clearly evident from Figs. 4a-b.

The location of the peak virus concentration undergoes change with time, as can be seen from Fig. 4c. Initially, the peak location remains in generation 22 for a certain period of time before advective transport results in the concentration increasing in the earlier generations. The peak location, as such, shifts to the earlier generations. The peak location once again shifts to the later generation after the advective clearance is complete.

### 3.3. Impact of different pertinent parameters

#### 3.3.1. Aerosol Peclet number

Peclet number for the aerosols ( $Pe_{ae}$ ) is defined as the ratio of advective transport of aerosols due to airflow and diffusive transport of the aerosols in air (see Eq. 9). The range of  $Pe_{ae}$  considered in this analysis is selected based on physiologically realistic air flow rate in the lungs and inhaled aerosol sizes.

A larger  $Pe_{ae}$  indicates a greater dominance of advective transport with respect to diffusive transport and vice-versa. Increase in  $Pe_{ae}$ , therefore, leads to the aerosols reaching deeper parts of the lung. As a consequence, a larger volume of aerosols are deposited in the deeper generations with increase in  $Pe_{ae}$ . This is clearly evident from Fig. 5a. This trend is, however, observed to be reversed i.e. the aerosol deposition tends to shift towards the earlier generations, when  $Pe_{ae}$  is increased beyond  $1.59 \times 10^9$ . At  $Pe_{ae} = 3.07 \times 10^{11}$ , maximum deposition is observed to occur in the first few generations with reducing deposition towards the deeper generations and almost no deposition in the deep lung (beyond  $N = 18$ ). Similar observations have been made in previous investigations as well [26]. The reason is due to a larger contribution of impact deposition of the aerosols in the earlier generations at such high  $Pe_{ae}$ . Diffusional and sedimentation deposition dominates over impact deposition at relatively lower  $Pe_{ae}$ .

Figures 5(b-c) shows the virus concentration in the mucus for different  $Pe_{ae}$  at the end of aerosol deposition ( $\tau = 5$ ) and at  $\tau = 10000$ . Wide variation in virus concentration for different  $Pe_{ae}$  makes it difficult to present all the plots in a single figure and as such, the plots are subdivided into two separate figures. Virus concentrations for  $Pe_{ae}$  from  $2.54 \times 10^7$  to  $1.59 \times 10^9$  are shown in Fig. 5b, while those beyond  $1.59 \times 10^9$  are shown in Fig. 5c. It can be observed from both these plots that the virus concentration at the end of deposition (i.e. at  $\tau = 5$ ) follows the aerosol deposition patterns as shown in Fig. 5a. Interestingly, washout of the virus deposited in the mucus does not undergo any significant change with variation in  $Pe_{ae}$ , as evident from Figs. 5b-d. However, location of virus deposition has an important impact on its washout. Viruses deposited before generation 18 gets washed out quickly due to the advection-dominated mucus clearance in that region. Viruses deposited beyond generation 18, however, gets transported much slowly due to the weak diffusive transport occurring in that region. Viruses deposited at very large  $Pe_{ae}$  ( $\sim 3.07 \times 10^{11}$ ) are, therefore, washed out of the lungs relatively quickly since majority of the deposition takes place before generation 18. In case of lower  $Pe_{ae}$ , however, the deposited viruses continue to persist in the deep lung (beyond  $N = 18$ ) even though advection washes out the deposited virus from the earlier generations. Temporal change in the peak location with  $Pe_{ae}$ , shown in Fig. 5e, also highlights this effect.

#### 3.3.2. Airway Strouhal number

Strouhal number for the airways ( $St_a$ ) is defined in this analysis as the ratio of convective airflow time scale to the breathing time scale. Physiological considerations result in  $St_a$  varying between 0.001 and 0.1. The same is taken as the range of study in this analysis.

An increase in  $St_a$  can be the result of an increase in the convective airflow time scale (which translates to a reduced airflow velocity) or a reduction in  $T_b$ , and vice-versa. In either case, this results in decreasing amount of aerosols being inhaled and the concentration front progression into the lung progressively decreasing. Consequently, smaller amounts of aerosol are deposited in the mucus and the deposition also tends to shift towards the upper airways with increase in  $St_a$ . The change in deposition with variation in  $St_a$ , as shown in Fig. 6a, adequately highlights this. Reducing aerosol deposition with increase in  $St_a$  results in decreasing virus concentration as well. This is evident from a comparison of virus concentration for different  $St_a$  in Fig. 6b. Qualitative nature of the curves remain similar to the deposition patterns shown in Fig. 6a. Any

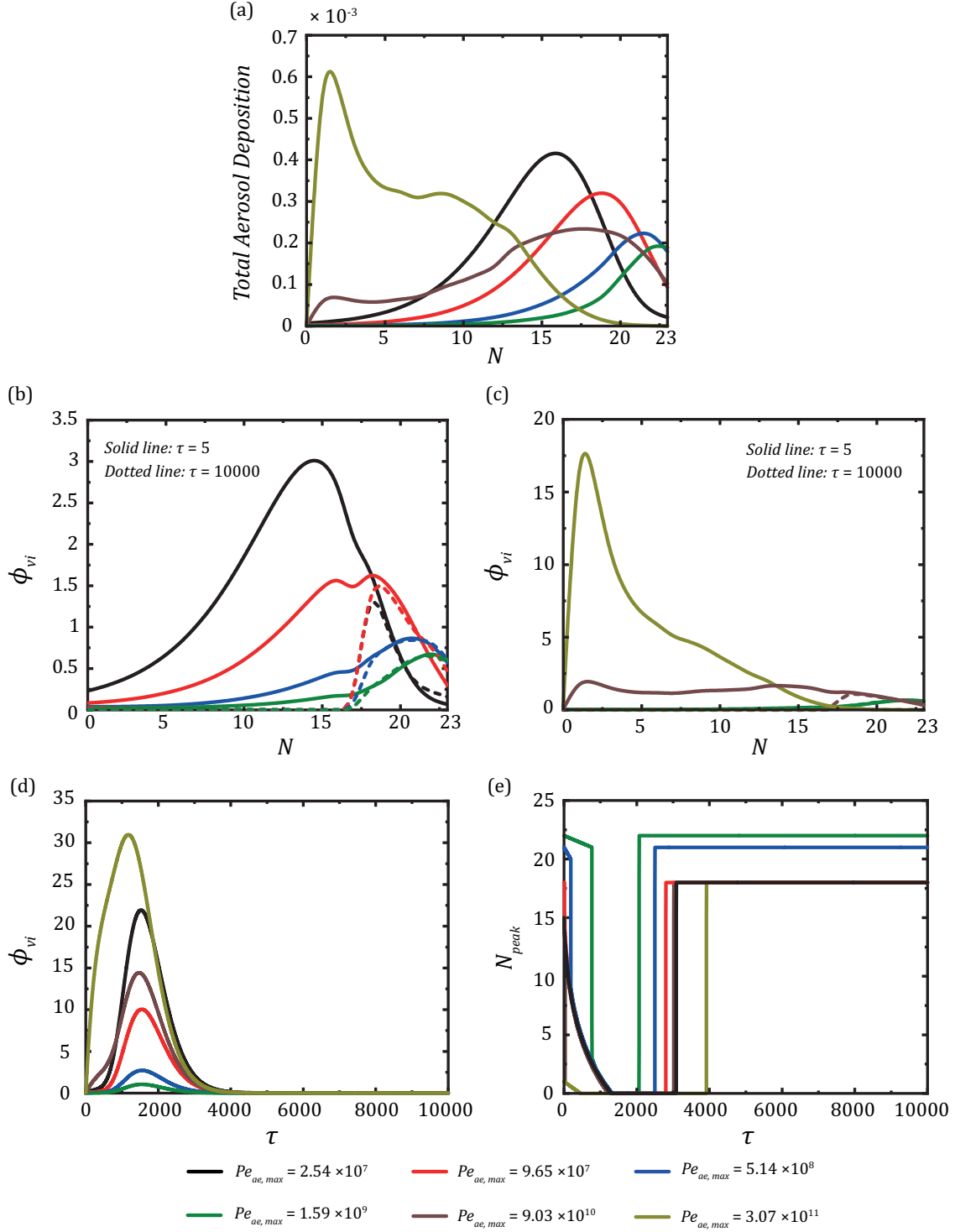


Figure 5: (a) Aerosol deposition within the lung for different  $Pe_{ae}$  (b) Virus concentration within the lung at  $\tau = 5$  and  $\tau = 10000$  for  $Pe_{ae}$  from  $2.54 \times 10^7$  to  $1.59 \times 10^9$  (c) Virus concentration within the lung at  $\tau = 5$  and  $\tau = 10000$  beyond  $1.59 \times 10^9$  (d) Temporal change in virus concentration at  $N = 0$  for different  $Pe_{ae}$  (e) Temporal change in location of maximum virus concentration within the lung for different  $Pe_{ae}$ .

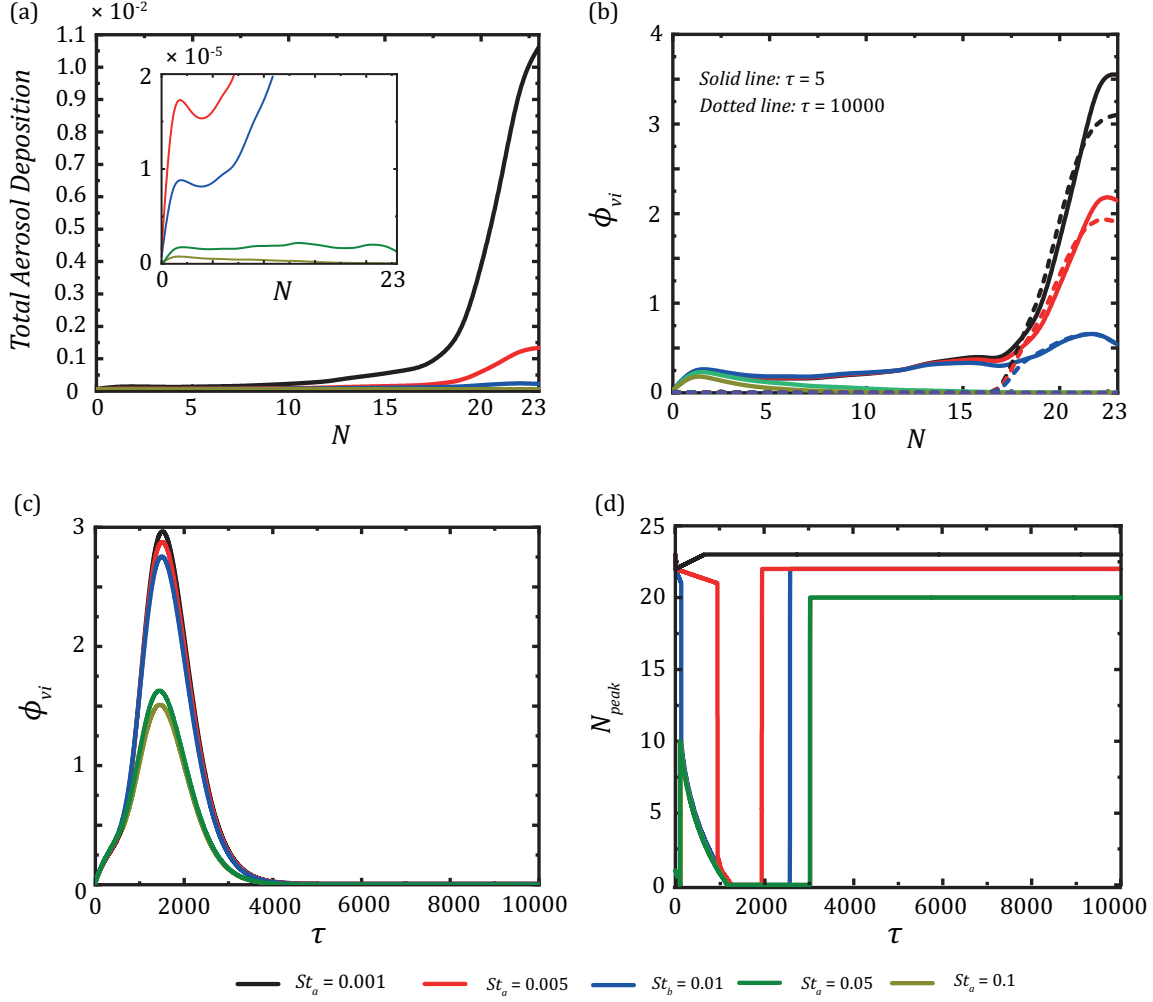


Figure 6: (a) Aerosol deposition within the lung for different  $St_a$  (b) Virus concentration within the lung for different  $St_a$  at  $\tau = 5$  and  $\tau = 10000$  (c) Temporal change in virus concentration at  $N = 0$  (d) Temporal change in location of maximum virus concentration within the lung.

change in  $St_a$ , however, do not affect the mucus clearance rate from the lung or diffusivity of the virus in mucus. Virus washout from the lung, therefore, remains unaffected when  $St_a$  is changing, as shown from the temporal change of virus concentration at  $N = 0$  in Fig. 6c.

Figure 6d indicates the temporal change in location of maximum virus concentration within the lung for different  $St_a$ . It can be observed that for the smallest  $St_a$  the peak location remains in the deep lung (generations 21, 22) throughout. In the other cases, the peak location shifts from the initial deposition peak towards the earlier generations and then shifts back to the deep lung, indicating the presence of residual virus in the deep lung even after washout from the earlier generations is complete. This is also evident from the virus concentrations at  $\tau = 10000$  in Fig. 6b.

### 3.3.3. Virus Peclet number

$Pe_{vi}$  represents the relative dominance of advective transport in the mucus layer and diffusive transport of the viruses in the mucus (see Eq. 42). The range of  $Pe_{vi}$  considered in this study ( $4.56 \times 10^7 - 4.56 \times 10^8$ ) is chosen based on the reported size of SARS-CoV2 virus (10 – 100 nm) and the advective clearance rate of mucus in a human lung.

An increase in  $Pe_{vi}$  indicates a larger impact of advection (or a smaller impact of diffusion) on the

overall transport and vice-versa. The change in  $Pe_{vi}$  considered in this analysis, however, is not large enough to cause significant alterations in the virus transport rate. This is evident from Fig.7a which shows the virus concentration within the lung for the two extreme  $Pe_{vi}$  considered in this analysis, at the end of aerosol deposition ( $\tau = 5$ ) as well as at  $\tau = 10000$ . It can be observed that at both time instances the virus concentrations for the two  $Pe_{vi}$  overlap each other indicating that the transport rates remain almost invariant. A closer look, however, reveals that the virus concentrations for the two extreme cases differ from each other in the deep lung (beyond  $N = 18$ ) at  $\tau = 10000$ . The reason for such difference is the faster diffusive transport taking place at the lower  $Pe_{vi}$ .

Virus washout curves at  $N = 0$  and  $N = 23$ , as shown in Fig. 6c, corroborate the above inferences. As expected, the change in peak location with time remains almost similar for the two cases with only a small time delay between them (see Fig. 6d).

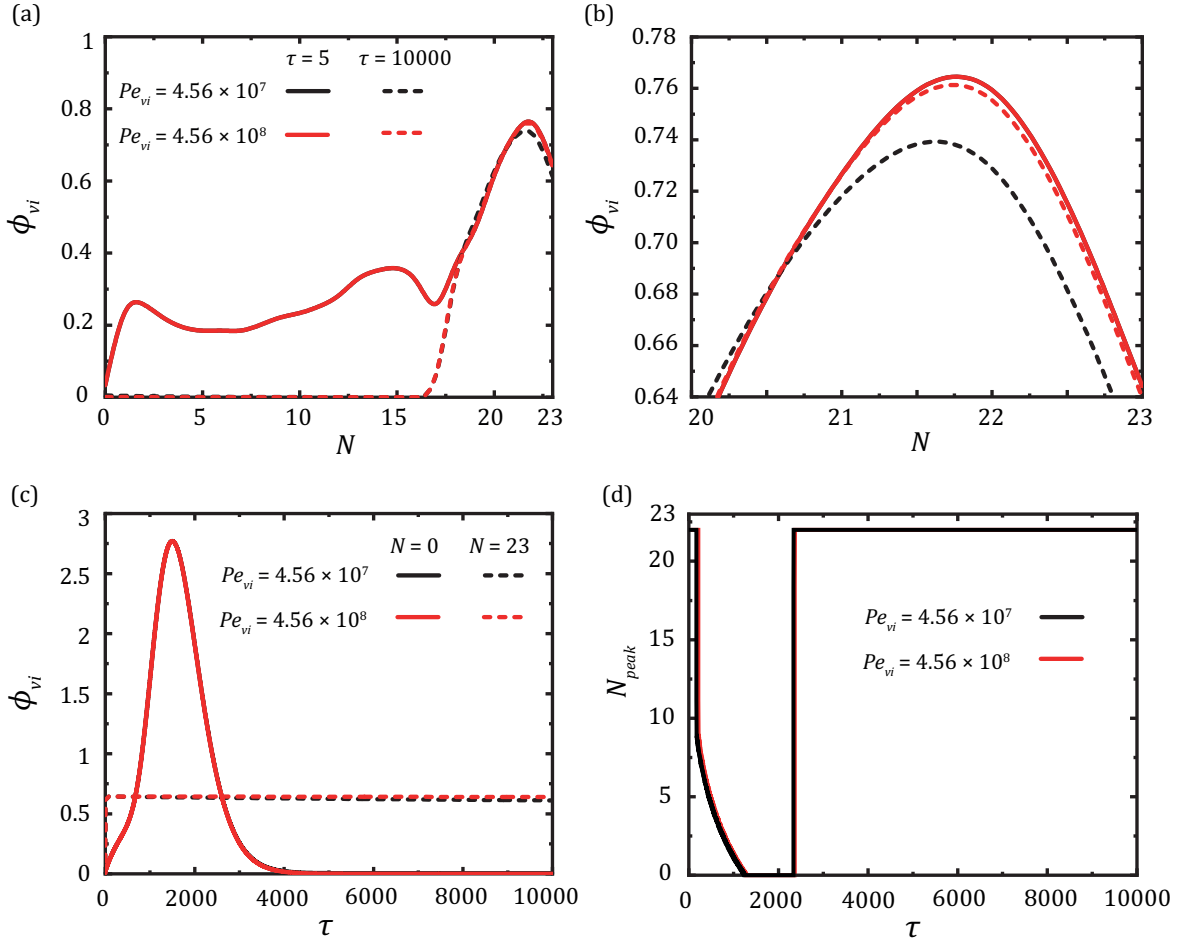


Figure 7: (a) Virus concentration within the lung at the end of deposition ( $\tau = 5$ ) and at  $\tau = 10000$  for two different  $Pe_{vi}$ . A zoomed view is shown in (b) to clearly illustrate the difference in the concentration in the deep lung. (c) Temporal change in virus concentration at the  $0^{th}$  generation for different  $Pe_{vi}$  (d) Change in location of virus concentration peak within the lung with time for different  $Pe_{vi}$

### 3.3.4. Mucus Strouhal number

Strouhal number in the mucus layer ( $St_m$ ) is defined as the ratio of the advective time scale in the mucus layer to the breathing time scale. A larger  $St_m$ , therefore, indicates a longer advective time scale which suggests a slower advective clearance of mucus from the lung and vice-versa. Physiologically,  $St_m$  is estimated to vary between 180 and 1440 depending on the breathing time scale, with approximately 360 for



a normal breathing time of 4s. Keeping this in mind, the range of  $St_m$  variation is considered to be from 100 to 1500 in this analysis.

Figure 8a represents the virus concentration in the mucus layer at the end of aerosol deposition for various  $St_m$ . It can be observed that there is no significant difference between the virus concentrations when  $St_m$  remains large. It is only when  $St_m$  becomes  $\sim 300$  and lower that deviations become apparent enough. The reason for these deviations is much faster mucus clearance at low  $St_m$  which is able to transport the deposited viruses away from the initial deposition location even before the deposition is complete.

Faster clearance of mucus and hence, viruses out of the lung is apparent from the virus washout curves and the peak location change with time for different  $St_m$  as shown in Fig. 8b and Fig. 8c, respectively.

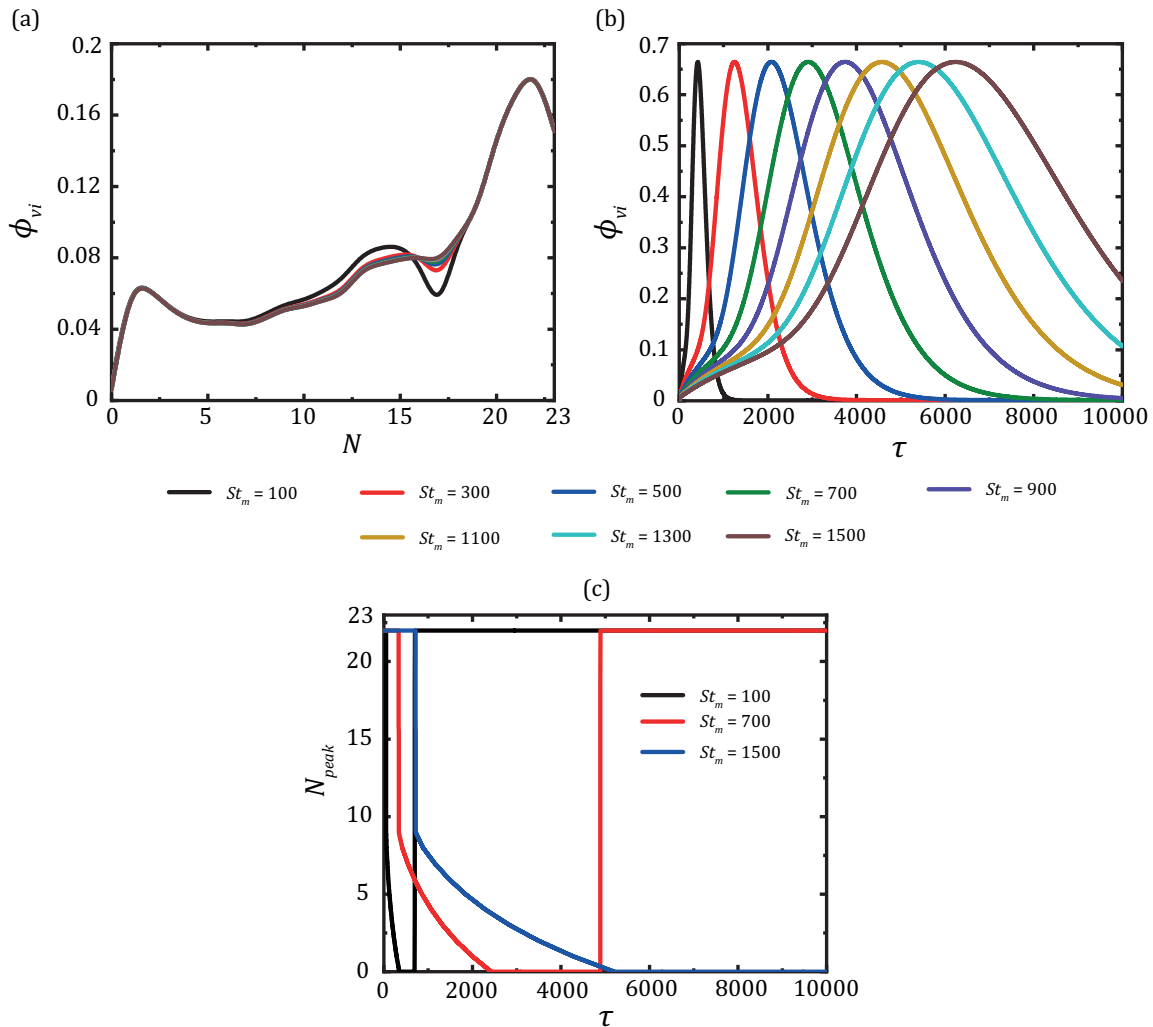


Figure 8: (a) Virus concentration within the lungs at the end of aerosol deposition for various  $St_m$  (b) Temporal change of virus concentration at the  $0^{th}$  generation of the lung for various  $St_m$  (c) Change in location of virus concentration peak within the lung for  $St_m = 100, 700, 1500$

### 3.3.5. Exposure duration

The time duration for which an individual is exposed to the virus-laden aerosols is another important parameter affecting virus transport within the lungs. The impact of exposure duration ( $\tau_{exp}$ ) on virus transport is studied by varying the number of breathing cycles for which the aerosols are inhaled into the lungs.

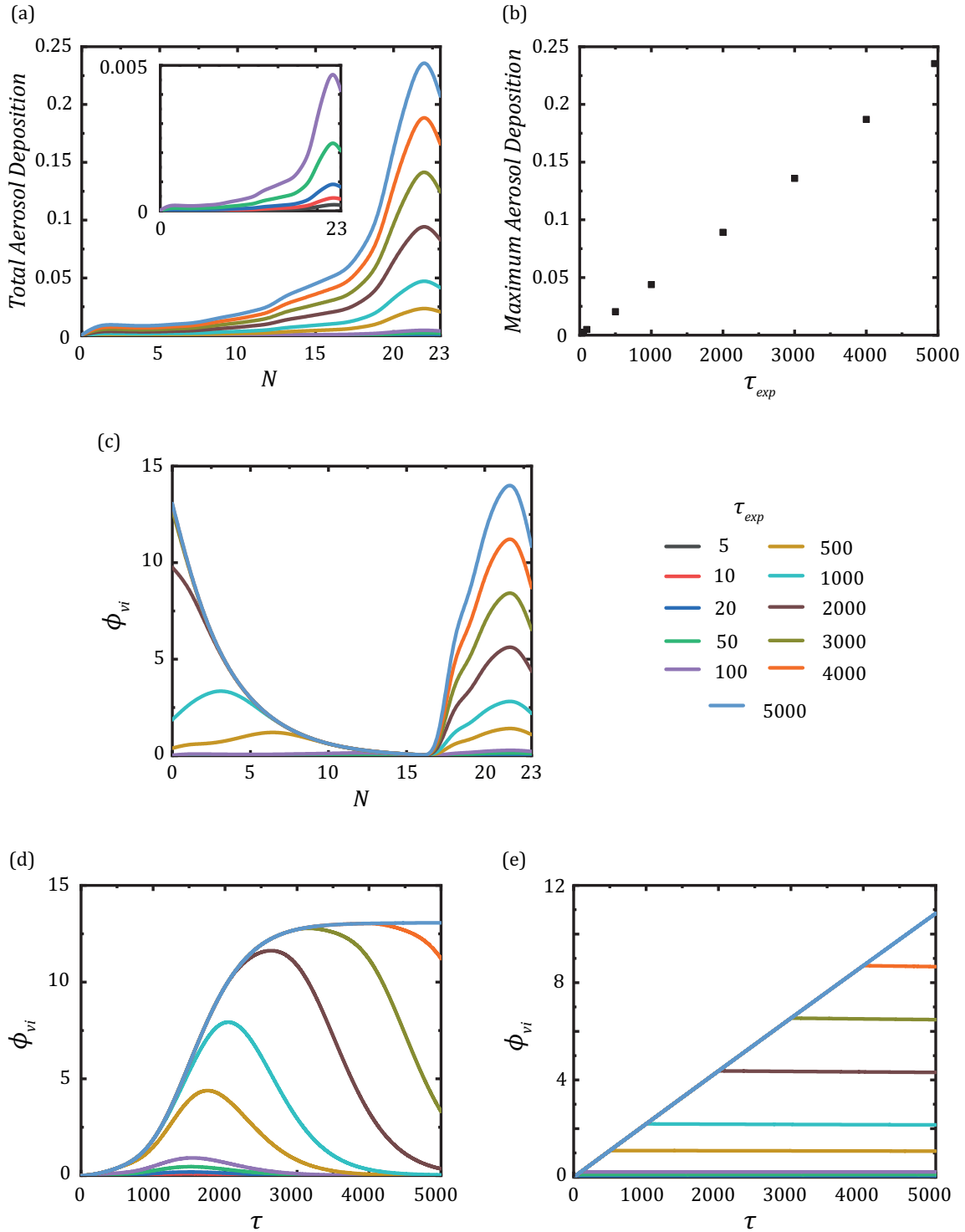


Figure 9: (a) Total aerosol deposition in the airway mucus with lung generation for different  $\tau_{exp}$ . Deposition for  $\tau_{exp} = 5 - 100$  is shown as inset (b) Variation in maximum aerosol deposition magnitude with change in  $\tau_{exp}$  (c) Virus concentration within the lungs for different  $\tau_{exp}$  (d) Temporal variation of virus concentration at  $0^{th}$  generation for different  $\tau_{exp}$  (e) Temporal variation of virus concentration at  $23^{rd}$  generation for different  $\tau_{exp}$

Figure 9a shows the total amount of aerosols deposited in the airway mucus for various  $\tau_{exp}$  considered in this analysis. It can be observed that while the deposition pattern within the lungs remain almost identical, the magnitude of deposition increases as  $\tau_{exp}$  become longer. It is also noted that this increase in deposition magnitude with  $\tau_{exp}$  has a nearly linear nature, as shown in Fig. 9b.

Figure 9c shows the virus concentration within the lungs for various  $\tau_{exp}$  at the end of respective exposures. As expected, the virus concentration also increases as  $\tau_{exp}$  becomes longer as a result of the larger aerosol deposition. This is clearly evident from a comparison of the virus concentrations in the deep lung ( $N = 18$  onwards), where advective mucus clearance due to mucociliary transport is absent. In the upper airways (before  $N = 18$ ), mucus advective clearance occurs simultaneously with aerosol deposition and as such, the effective virus concentration is the resultant of virus transport due to the deposition and clearance mechanisms. While virus concentration increases in these generations due to higher aerosol deposition, continuous mucus advection clears the high virus concentrations from these generations towards the  $0^{th}$  generation and as a consequence, the virus accumulates in the first few generations leading to much higher virus concentration.

Temporal variations of virus concentration at the two extremities i.e. the  $0^{th}$  and the  $23^{rd}$  generations, in Figs. 9(d-e) confirms the above inference. It is also observed that the virus concentration at both extremities continue to increase till aerosol inhalation ends. Beyond that time, the virus concentration decreases in the  $0^{th}$  generation indicating virus washout from the lung. This decrease is, however, much slower in the  $23^{rd}$  generation due to the absence of advective mucus clearance.

## 4. Discussion

It is a known fact that clinical complications arise as a result of exposure to respiratory viruses (such as SARS-CoV2). People exposed to such viruses remain asymptomatic or mildly symptomatic in certain cases, while pneumonia-like symptoms and associated complications are also possible. One possible cause for such varied nature of the symptoms is the location where viruses are deposited within the lung. It is probable that deep lung depositions of the viruses result in more complicated clinical symptoms, while upper lung and nasopharyngeal depositions present with more subdued health effects.

Results presented in Section 3 show that viruses deposited before the  $18^{th}$  lung generation is cleared out of the lung at a much faster rate, as compared to viruses that are deposited in the deep lung ( $18^{th}$  generation onwards). The primary reason for such difference in the clearance rate is the contribution of mucus advective motion arising due to ciliary beating, which remains absent after the  $18^{th}$  lung generation. Mucus clearance and hence, virus washout from the lung remains advection-dominated up to the  $18^{th}$  lung generation and diffusion-dominated after  $18^{th}$  lung generation. Since mucus advection is much stronger than virus diffusion in the mucus, the clearance rate is also much faster from the advection-dominated regions. As such, if virus deposition takes place in the deep lung or the viruses somehow reach the deep lung, it will continue to persist in the lung for a very long period of time.

It is, thus, critical to not only understand the conditions under which the virus can reach the deep lung, but to also explore the means to enhance virus clearance from the lung. These are discussed in the following sections using the results presented in Section 3.

### 4.1. Virus deposition in the lung

The analysis carried out in Section 3 have established that the spatial distribution of virus in the lungs - at the end of exposure - qualitatively follows the aerosol deposition pattern. It is also observed that the main parameters determining the spatial distribution of aerosol deposition in the lungs are  $Pe_{ae,max}$  and  $St_a$ . Figure 10 plots the ratio of aerosols deposited in the deep lung to the aerosols deposited in the lung as a function of  $Pe_{ae,max}$  and  $St_a$ .

A considerable fraction of the aerosols ( $\sim 50\%$ ) are observed to be deposited in the deep lung when  $Pe_{ae,max}$  remains larger than  $2.54 \times 10^7$ . This fraction increases to  $\sim 75\%$  ( $Pe_{ae,max} = 9.65 \times 10^7$ ) before decreasing to  $\sim 13\%$  ( $Pe_{ae,max} = 7.18 \times 10^9$ ). A second increase in the deep lung deposition is observed when  $Pe_{ae,max}$  is further increased to  $7.18 \times 10^9$  ( $\sim 50\%$ ) and then it again decreases to become negligible ( $< 1\%$ ) beyond  $Pe_{ae,max} = 3.07 \times 10^{11}$ . Deep lung deposition of the aerosols can, thus, be avoided when  $Pe_{ae,max}$  remains larger than  $3.07 \times 10^{11}$  or less than  $2.37 \times 10^6$ . These  $Pe_{ae,max}$  values translate to a aerosol droplet size of  $10 \mu\text{m}$  and  $0.003 \mu\text{m}$ , respectively, considering normal breathing in a healthy individual (tidal

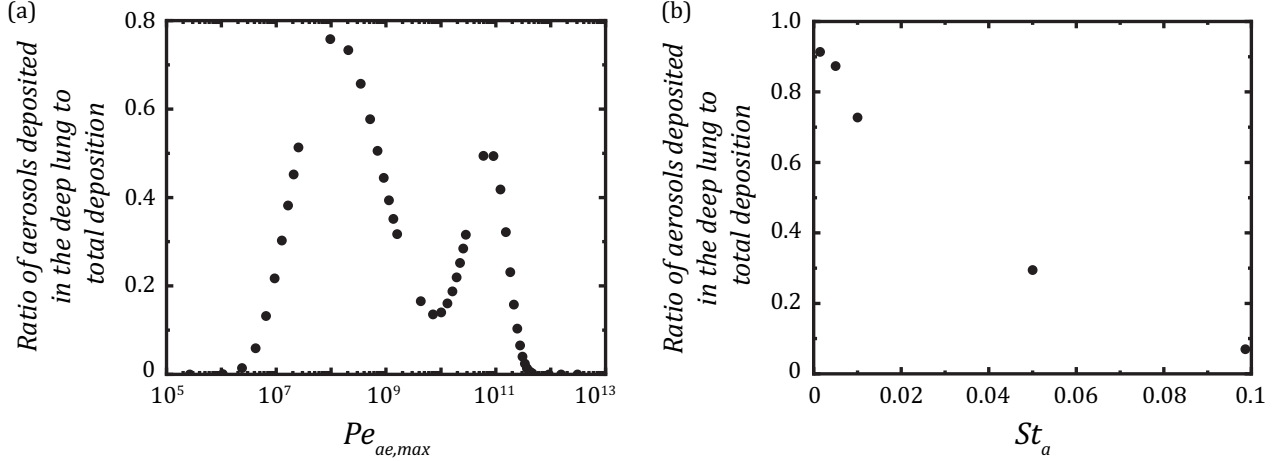


Figure 10: Change in ratio of the aerosols deposited in the deep lung to the total aerosol deposition within the whole lung with (a)  $Pe_{ae,max}$  and (b)  $St_a$

volume of 1000 ml and a breathing period of 4s). Deep lung deposition can also be minimised if  $Pe_{ae,max}$  remains in the range of  $4.29 \times 10^9 - 1.6 \times 10^{10}$  (corresponding aerosol droplet sizes of  $0.2 - 0.6 \mu\text{m}$ ).

It can also be observed from Fig. 10b that deep lung deposition of the aerosols reduce with increase in  $St_a$ . As discussed, increase in  $St_a$  is possible either when the breathing time scale becomes shorter or the convective time scale becomes longer (inhalation flow velocity becomes smaller). It can, thus, be stated that faster breathing (i.e. shorter breathing time) or shallow breaths can help in reducing deep lung deposition. It is also observed that exposure duration has a significant influence on deposition of the virus-laden aerosols within the lungs. Deposition increases with exposure duration and hence, it is essential to minimise exposure in order to reduce deposition of viruses in the lung.

#### 4.2. Virus washout from the lung

Once the virus gets deposited within the lung, the most critical aspect is to ensure quick washout of the viruses from the lung. Analysis have established that virus washout from the lung is dependent on  $Pe_{vi}$  and  $St_m$ . It is observed that virus washout from the lung is enhanced when both  $Pe_{vi}$  and  $St_m$  decreases, the enhancement with  $St_m$  being substantially larger.

Change in  $Pe_{vi}$ , keeping all other parameters fixed, suggests a change in diffusivity of virus in the mucus layer (see Section ??). Virus diffusivity does not influence mucus advection in any form and as such, it is observed that virus clearance from the upper airways (before the 18<sup>th</sup> generation) remains almost similar with change in  $Pe_{vi}$ . Virus clearance in the diffusion-dominated deep lung is, however, observed to become marginally slower when  $Pe_{vi}$  increases (i.e. virus diffusivity reduces). It can, thus, be seen that virus diffusivity in the mucus layer plays an important role in determining its clearance from the deep lung. Diffusivity of the virus is determined by its inverse dependence on virus size and viscosity of the mucus layer (see Eq.). A smaller virus size and lower viscosity of the mucus layer, as such, promotes faster virus clearance from the lung from the fluid mechanics perspective. While virus size cannot be controlled, mucus property modification is viable and can be a possible approach in enhancing virus clearance from the deep lung.

$St_m$  is observed to mainly influence virus clearance from the advection-dominated region of the lung i.e. before generation 18, while it has no impact on virus clearance from the deep lung. It is observed that an increase in  $St_m$  - which indicates longer mucus advection time-scale (smaller advective velocity) or a faster breathing time - impairs virus clearance from the upper airways. A larger mucus advective velocity and a slower breathing process, therefore, promotes virus clearance from the upper airways.

#### 4.3. Hypothesis on secondary transport of deposited viruses

The conditions (aerosol droplet size, flow rate, breathing period) which promotes deep lung deposition of virus is discussed in Section 4.1. However, it is also possible that viruses that are deposited in the upper airways or the naso-pharyngeal region are transported towards the deep lung.

One possible mechanism of this secondary transport of the deposited viruses is due to aerosolisation of the mucus. The mucus lining the airways is a highly viscous fluid and as such, does not aerosolise easily. However, in case of imbalance in the mucus clearance rate, mucus buildup is possible in the upper airways. One possible cause of imbalance in the mucus clearance is due to irregular ciliary beating - spatially or temporally - or complete impairment of the beating mechanism. Several other factors can also result in these imbalances. The mucus layer thickens due to such imbalances which reduces the air flow passage in the airways. This promotes aerosolisation of the mucus. The flow passage reduction can also be a result of other clinical issues (such as asthma). In either case, the flow passage constriction can also result in air flow blockages in extreme cases and introduce violent breakup of the mucus layer. The resulting aerosol droplets, if they are of the right size, can travel towards and potentially reach the deep lung.

The other mechanism by which the deposited viruses can reach the deep lung is diffusion through the mucus layer itself. This is possible only if the advective mucus clearance is completely absent. Such a situation can be encountered due to complete impairment of the ciliary beating mechanism which controls the advective mucus clearance. While this promotes re-aerosolisation of the mucus (as already discussed), it is improbable that the virus will be able to diffuse across the large length required to reach the deep lung. The total length of a typical healthy human lung is  $\sim 0.28$  m, while viruses typically have diffusivity  $\sim \mathcal{O}(10^{-13} \text{ m}^2/\text{s})$ . However, diffusion through short distances within the lung remains a possibility.

## 5. Summary

A coupled mathematical model of aerosol and virus transport is developed considering a one-dimensional Weibel-like *trumpet* idealisation of the lung geometry. Virus-laden aerosols are assumed to be inhaled into the lungs for specific exposure durations. The aerosols are transported in the lungs along with the airflow and then deposit in the respiratory mucus through different mechanisms. The deposited viruses are transported within the mucus by a combined action of virus diffusion and mucociliary clearance.

The analysis is carried out in a dimensionless manner and the results are quantified in terms of relevant dimensionless parameters. It is observed that viruses deposited in the upper respiratory tract (before 17<sup>th</sup> generation) are washed out relatively faster due to dominance of mucociliary clearance in this region. Absence of mucociliary clearance in the deep lung (before 17<sup>th</sup> generation) results in purely diffusive transport of viruses leading to significantly slower virus clearance from the deep lung. The region of the lung where the virus-laden aerosols are deposited, as such, has an important influence on clearance of the viruses from the lung. Exposure duration is also observed to have a significant influence on deposition of the virus-laden aerosols with deposition increasing with exposure duration. It is, therefore, essential to minimise exposure of an individual to reduce the risk of an infection.

Deep lung deposition of the aerosols is observed to take place for a specific range of  $Pe_{ae}$ . This corresponds to aerosol sizes of  $0.003 \mu\text{m}$  to  $10 \mu\text{m}$  for normal breathing. It is also observed that deep lung deposition is enhanced with decrease in  $St_a$  which translates to slower breathing and deep breaths. A reduction in  $Pe_{vi}$  is observed to marginally enhance virus clearance from the deep lung due to larger virus diffusivity, although it does not have much influence in virus clearance from the upper respiratory tract. The latter is observed to be enhanced with reduction in  $St_m$  which suggests that a larger mucus velocity or a slower breathing process promotes virus clearance from the upper respiratory tract.

## Acknowledgements

The authors gratefully acknowledge the grant provided by MHRD, Govt. of India under the SPARC programme (Project Code: P838).

## References

- [1] W. J. Wiersinga, A. Rhodes, A. C. Cheng, S. J. Peacock, H. C. Prescott, Pathophysiology, transmission, diagnosis, and treatment of coronavirus disease 2019 (covid-19): a review, *Jama* 324 (8) (2020) 782–793.
- [2] R. Mittal, R. Ni, J.-H. Seo, The flow physics of covid-19, *Journal of Fluid Mechanics* 894 (2020) F2. doi:10.1017/jfm.2020.330.

- [3] C. Quirouette, N. P. Younis, M. B. Reddy, C. A. Beauchemin, A mathematical model describing the localization and spread of influenza a virus infection within the human respiratory tract, *PLOS Computational Biology* 16 (4) (2020) e1007705.
- [4] A. Guha, Transport and deposition of particles in turbulent and laminar flow, *Annu. Rev. Fluid Mech.* 40 (2008) 311–341.
- [5] W. Hofmann, Modelling inhaled particle deposition in the human lung—a review, *Journal of Aerosol Science* 42 (10) (2011) 693–724.
- [6] A. Chakravarty, N. A. Patankar, M. V. Panchagnula, Aerosol transport in a breathing alveolus, *Physics of Fluids* 31 (12) (2019) 121901.
- [7] R. Fishler, P. Hofemeier, Y. Etzion, Y. Dubowski, J. Sznitman, Particle dynamics and deposition in true-scale pulmonary acinar models, *Scientific reports* 5 (2015) 14071.
- [8] P. Koullapis, P. Hofemeier, J. Sznitman, S. C. Kassinos, An efficient computational fluid-particle dynamics method to predict deposition in a simplified approximation of the deep lung, *European Journal of Pharmaceutical Sciences* 113 (2018) 132–144.
- [9] M. Bailey, E. Ansoberlo, R. Guilmette, F. Paquet, Updating the icrp human respiratory tract model, *Radiation protection dosimetry* 127 (1-4) (2007) 31–34.
- [10] D. B. Taulbee, C. Yu, A theory of aerosol deposition in the human respiratory tract, *Journal of Applied Physiology* 38 (1) (1975) 77–85.
- [11] S. K. Devi, M. V. Panchagnula, M. Alladi, Designing aerosol size distribution to minimize inter-subject variability of alveolar deposition, *Journal of Aerosol Science* 101 (2016) 144–155.
- [12] E. R. Weibel, A. F. Cournand, D. W. Richards, *Morphometry of the human lung*, Vol. 1, Springer, 1963.
- [13] H.-C. Yeh, G. Schum, Models of human lung airways and their application to inhaled particle deposition, *Bulletin of mathematical biology* 42 (3) (1980) 461–480.
- [14] K. Horsfield, G. Cumming, Morphology of the bronchial tree in man., *Journal of applied physiology* 24 (3) (1968) 373–383.
- [15] D. Smith, E. Gaffney, J. Blake, Modelling mucociliary clearance, *Respiratory physiology & neurobiology* 163 (1-3) (2008) 178–188.
- [16] C. Karamaoun, B. Sobac, B. Mauroy, A. Van Muylem, B. Haut, New insights into the mechanisms controlling the bronchial mucus balance, *PloS one* 13 (6) (2018) e0199319.
- [17] A. Handel, L. E. Liao, C. A. Beauchemin, Progress and trends in mathematical modelling of influenza a virus infections, *Current Opinion in Systems Biology* 12 (2018) 30–36.
- [18] A. L. Bauer, C. A. Beauchemin, A. S. Perelson, Agent-based modeling of host–pathogen systems: The successes and challenges, *Information sciences* 179 (10) (2009) 1379–1389.
- [19] M. A. Jensen, Y.-Y. Wang, S. K. Lai, M. G. Forest, S. A. McKinley, Antibody-mediated immobilization of virions in mucus, *Bulletin of mathematical biology* 81 (10) (2019) 4069–4099.
- [20] L. Junqueira, J. Carneiro, R. Kelley, *Basic histology*, 9th edition, Stamford, Conn.: Appleton & Lange, 1998.
- [21] B. Mauroy, C. Fausser, D. Pelca, J. Merckx, P. Flaud, Toward the modeling of mucus draining from the human lung: role of the geometry of the airway tree, *Physical biology* 8 (5) (2011) 056006.
- [22] S. G. K. Devi, Aerosol deposition studies in human lung - towards personalized medicine, Ph.D. thesis, IIT Madras, India (2018).

- [23] C. Darquenne, M. Paiva, One-dimensional simulation of aerosol transport and deposition in the human lung, *Journal of applied physiology* 77 (6) (1994) 2889–2898.
- [24] C. Mitsakou, C. Helmis, C. Housiadas, Eulerian modelling of lung deposition with sectional representation of aerosol dynamics, *Journal of Aerosol Science* 36 (1) (2005) 75–94.
- [25] J. Heyder, J. Gebhart, G. Rudolf, C. F. Schiller, W. Stahlhofen, Deposition of particles in the human respiratory tract in the size range 0.005–15  $\mu\text{m}$ , *Journal of aerosol science* 17 (5) (1986) 811–825.
- [26] J.-I. Choi, C. S. Kim, Mathematical analysis of particle deposition in human lungs: an improved single path transport model, *Inhalation toxicology* 19 (11) (2007) 925–939.